The tendon differentiation program is activated in human adipose stromal cells embedded in a 3D-collagen matrix

Maxime Hordé[a], Jonathan Fouchard[a], Xavier Laffray[b], Cédrine Blavet[a], Véronique Béréziat[c], Claire Lagathu[c], Ludovic Gaut [a], Delphine Duprez[a,1,#] and Emmanuelle Havis[a,1,#]

[a] Sorbonne Université, Institut Biologie Paris Seine, CNRS UMR7622, Developmental Biology Laboratory, Inserm U1156, F-75005 Paris, France

[b] Université Paris Est Creteil, Glycobiology, Cell Growth and Tissue Repair Research Unit (Gly-CRRET), EA 4397, F-94010 Creteil, France.

[c] Sorbonne Université, Inserm UMRS938, Centre de Recherche Saint-Antoine (CRSA), Institut Hospitalo-Universitaire de Cardio-Métabolisme et Nutrition (ICAN), F-75012 Paris, France

[1] Co-senior authors; [#] Co-corresponding authors

Key words: tendon differentiation program, tendon-associated matrix, viscoelastic properties, human adipose stromal cells, 3D-culture system

Abstract

During development, tendon cell differentiation relies on molecular and mechanical parameters that control the expression of tendon collagen and associated extracellular matrix proteins. However, the minimal cues able to initiate tendon differentiation from progenitor cells remains unknown. We analysed the molecular and mechanical parameters associated with tendon differentiation in human adipose stromal cells (hASCs) in a 3D-culture system. We generated 3D-hASC constructs by embedding hASCs in a type-I collagen gel under a static uniaxial geometrical constraint with no additional molecular and mechanical cues, and assessed tendon matrix gene expression and mechanical properties for up to three weeks in culture. Analysis of tendon matrix genes revealed a molecular progression consistent with the acquisition of a tendon phenotype. The analysis of viscoelastic properties of 3D-hASC constructs by nano-indentation indicated a progressive increase in tissue stiffness up to 10 kPa, concomitant with a reduced stress relaxation indicative of solid-like mechanical properties. These changes in mechanical properties were associated with transcription of tendon matrix components. In summary, we have established that hASCs cultured in 3D-system with minimal mechanical cues progress into the tendon differentiation program associated with variations of mechanical properties reminiscent of embryonic tendon development.

Introduction

How a progenitor cell differentiates via the tendon lineage is not fully understood. The molecular and mechanical cues regulating the tendon program have not been completely identified.

Tendon is a key component of the musculoskeletal system that transmits forces from muscle to bone to allow locomotion. To accomplish this function, tendons exhibit specific viscoelastic properties, with a Young's modulus much higher than other soft tissues [1,2]. Tendon is a connective tissue composed of tendon fibroblasts that produce a dense extracellular matrix (ECM) consisting mainly of type I collagen fibrils that display a specific spatial organisation to resist the tensile forces generated by muscle contraction. Compared to other components of the musculoskeletal system, little is known about the mechanisms involved in tendon cell differentiation from undifferentiated cells. There is no identified master gene for the tendon lineage. The tendon program is difficult to follow because of the lack of recognized markers for each step of the tendon differentiation program [3]. Moreover, developmental tendon fibroblast populations are not well characterized and the molecular markers of tendon cell populations are not well identified [4].

In vertebrates, type I collagen, encoded by *COL1A1* and *COL1A2* genes, is the main structural and functional component of tendons. The regulation of *COL1A1* transcription is under the control of several transcription factors at different stages of tendon formation. The main developmental tendon marker, the bHLH transcription factor Scleraxis (SCX) [5] regulates *COL1A1* transcription during development [6]. Two other transcription factors have been shown to regulate *COL1A1* transcription in adult mouse tendons, EGR1 [7] and MKX (Mohawk) [8,9]. In addition to *COL1A1* regulation, SCX is required and sufficient for the expression of the transmembrane glycoprotein *TNMD* (Tenomodulin) in developing limb tendons and tendon cell cultures [6,10,11]; TNMD being involved in tenocyte proliferation and tendon collagen fibril maturation in new-born mice [12,13]. This indicates that SCX acts as a starter of the tendon program, although not being a master gene for the tendon lineage. Tendons are still observed in *Scx* mutant mice, however, force-transmitting tendons display severe alterations with disorganized matrix [6,14]. The transcriptomic analysis of *SCX*-positive cells during mouse limb tendon development provided us with a list of genes enriched in fetal tendon cells [15]. Although the function of all the 100 top genes have not been studied, when studied, gene function analyses show an involvement in tendon collagen fibrillogenesis; exampled with *THBS2*, coding for Thrombospondin 2 a secreted ECM glycoprotein [16], *COL6A3* encoding

79 the chainα3 of the non-fibrillar type VI collagen [17] and *COL14A1* encoding the chainα1 of
80 the FACIT (fibril-associated collagen with interrupted triple helices) [18]. Top 100 genes also
81 include various ECM proteins contributing to tendon biomechanical properties, such as the
82 small leucine-rich proteoglycan, DCN (Decorin) [19], the secreted matrix protein POSTN
83 (Periostin) [20,21], the collagen-bonding protein, DPT (Dermatopontin) [22–24] and the lysyl
84 oxidase enzyme LOX, which catalyzes collagens cross-linking of through oxidative
85 deamination of lysine residues [25]. All these tendon-associated molecules provide us with
86 molecular markers to assess the developmental tendon phenotype. In addition to molecular
87 cues, mechanical parameters are key for tendon development. Axial, head and limb tendon
88 development is stopped in the absence of muscle contraction in chicken and mouse models
89 [26,27].
90 Mesenchymal Stem Cells (MSCs) are a standard in the field of adult stem cell biology,
91 due to their high differentiation capacities in various cell lineages, including osteoblast,
92 adipocyte or chondrocyte. Although MSCs can also differentiate into the tendon lineage, the
93 progression into the tendon lineage is not completely understood. Tendon cell differentiation is
94 difficult to follow *in vitro*, since the tendon phenotype is not maintained in tendon 2D-cell
95 cultures. Stem cells require molecular stimuli to induce a tendon phenotype when cultured in
96 2D [7,28,29]. Compared to 2D-culture systems, 3D-culture systems are more favourable to
97 trigger tendon differentiation [29–31]. Human, rat, mouse and avian tendon fibroblasts have
98 been extensively used in 3D-culture systems to study collagen fibrillogenesis [32–37]. In a
99 fibrin 3D-culture system, chicken embryonic tendon cells were able to produce matrix genes
100 resembling to native tendons [38]. An alternative approach has been to use MSCs in 3D-culture
101 systems, which enable the study of the mechanisms by which the tendon lineage is initially
102 selected [31]. The tendon differentiation potential has been analysed in numerous MSC types,
103 such as bone marrow-derived Mesenchymal Stem Cells (bmMSCs), human Adipose-derived
104 Stromal Cells (hASCs), mouse MSCs (with the C3H10T1/2 cell line). However, these 3D-
105 culture systems made of MSCs require molecular cues [7,30,39–41] or mechanical loading
106 [7,42–45] to reach and maintain a tendon phenotype.
107
108 Here, we developed a 3D-culture system with hASCs in a type I collagen hydrogel
109 maintained between two anchor points to assess whether hASCs were capable of undergoing a
110 tendon differentiation program with no external molecular cues and mechanical stimulation for
111 three weeks. The increased expression of tendon genes, tendon-associated matrix genes,
112 combined with increased stiffness and reduced relaxation of 3D-hASC constructs, show that

hASCs are directed towards a tendon differentiation program. This shows that hASCs undergo towards a tendon phenotype in a minimal 3D-culture system with no external molecular or mechanical cues.

Results

Development of a 3D-culture system mimicking tendon formation from human Adipose Stromal Cells.

Since adipose tissue is an attractive alternative source of MSCs [46,47], we developed a 3D-culture system with hASCs isolated from the stromal vascular fraction of human adipose tissue collected after liposuction surgery [48,49]. Because collagen hydrogels recapitulate the native biophysical microenvironment of tendon tissues, we chose collagen hydrogel as biomaterial. During embryonic development, tendon primordia are high-cell-density linear structures anchored between bone and muscle in formation. To mimic tendon embryonic development, hASCs were homogenously embedded in a collagen gel deposited between two anchor points using the Flexcell technology (Supplementary Figure 1). This technology consists in a holder with 24 cylindrical moulds conferring a homogeneous and regular shape to the constructs. Each mould is perforated with vertical holes through which the vacuum is applied, allowing the silicon elastic surface of the well to acquire the shape of the mould (Fig.1A). At the extremities of each cylinder, two nylon anchor stems allowed the maintenance of static tension in each construct (Fig. 1A). After isolation and amplification, hASCs were embedded in a 3.5% bovine type I collagen solution and seeded between the two anchor stems. Vacuum was maintained for 2 hours to generate a construct of a cylindrical shape. 3D-hASC constructs (which we define as Day -2) were then left for 48 hours to allow cell development under static tension by condensing the surrounding matrix. 3D-constructs were analysed starting from this time point, defined as Day 0 (Fig. 1B). Once generated, the 3D-constructs were maintained under static conditions for 21 days (Fig. 1B). We did not apply external forces and the 3D-constructs were only subjected to the tension forces exerted between the two anchoring points. At Day 0, 3D-hASC constructs exhibited diameter values of 2.08+/-0.08 mm (Fig. 1D). The diameters of 3D-hASC constructs decreased drastically from Day 0 to Day 7 (0.67+/-0.02 mm at Day 7) and then displayed a slow decrease from Day 7 to Day 21 (0.59+/-0.02 mm at Day 14, 0.55+/-0.04 mm at Day 21) (Fig. 1D). Notably, because the length of the construct is fixed, we could estimate a volume reduction of 3D-constructs of about 15-fold in the course of the 21 Days of culture. 3D-no cell constructs not seeded with hASC exhibit constant diameter values during the 3 weeks of culture, 4.46+/-0.48 mm at Day 0, 4.41+/-0.45 mm at Day 7, 4.5+/-0.45 mm at Day 14 and 4.46+/-0.48 mm at

147 Day 21 (Supplementary Fig. 1D-E). Similarly, the cross-sectional areas of 3D-no cell constructs
148 remain constant and significantly higher than those of 3D-hASC constructs (Supplementary
149 Fig. 1F). The total number of cells in the constructs remained relatively stable between Day 0
150 and Day 21, with a slight increase at Day 7 and a slight decrease between Day 7 and Day 21
151 (Fig. 1D). We did not observe any apoptosis features between Day 7 and Day 14
152 (Supplementary Fig. 2).
153 At a cellular level, hASCs in this 3D-culture system displayed a fusiform shape and
154 spindle-shaped nuclei, aligned in the direction defined by the two anchor points (Fig. 1E),
155 reminiscent of cell organisation in native tendons, while hASCs exhibited a star shape in 2D
156 cultures (Supplementary Fig. 1B). In addition, cells progressively aligned along the tension axis
157 as the angle between the cell axis and the axis of the 3D-hASC constructs decreased throughout
158 culture (Fig. 1F). RT-qPCR analysis of the expression of the main tendon collagen *COL1A1*
159 show a progressive increase from Day 0 to Day 21 (Fig. 1G). In situ hybridization revealed that
160 *COL1A1* was highly expressed in tendon constructs until Day 14 (Fig. 1H-I). However, at Day
161 21, *COL1A1* appeared to be more highly expressed in central cells than in ring cells (Fig. 1I).
162 We used this 3D-culture system to analyse the tendon differentiation potential of hASCs.
163
164 *hASCs are prone to tendon differentiation in a 3D-culture system.*
165 In order to assess the tendon differentiation potential of hASCs cultured in the 3D-conditions
166 described above, we analysed tendon gene expression at the transcript levels with RT-qPCR
167 and in situ hybridization experiments. We started the analyse with recognized tendon markers
168 at different time points during the culture. The mRNA expression of the following genes was
169 first analysed: the recognized tendon markers *SCX*, *MKX*, *TNMD* and *THSB2*. *SCX* expression
170 was detected, although at low level, both by in situ hybridization and RT-qPCR (Fig. 2A-B).
171 *SCX* expression slightly increased up to Day 7, remained constant up to Day 14 and then
172 decreased up to Day 21 (Fig. 2A). *MKX* expression was not detected at Day 0 and Day 2, but
173 started to be expressed on Day 4 and increased up to Day 21 (Fig. 2C). Interestingly, *TNMD*
174 was expressed in all 3D-hASC constructs on Day 4 but was not detected or at low levels at the
175 other timepoints (Fig. 2D). *THBS2* mRNA expression was significantly increased during human
176 3D-hASCs construct development (Fig. 2E). We also analysed the expression of other genes
177 identified in the Top100 genes (ordered with the highest enrichment score) of *SCX*-positive
178 cells during mouse limb development [15], such as *TM4SF1* (Transmembrane 4 superfamily
179 member 1, ranked 4th), *ANXA1* (Annexin A1, ranked 19th) and *S100A10* (member of the S100
180 family of cytosolic Ca^{2+}-binding proteins, ranked 73rd). *TM4FS1* expression was detected from

181 Day 0 and increased significantly in 3D-hASC constructs overtime (Fig. 2G). In contrast,
182 *ANXA1* expression was first decreased at Day 2 and slightly increased at Day 21 (Fig. 2H). The
183 *S100A10* expression levels were stable in 3D-hASC constructs until Day 14 and slightly
184 decreased between Day 14 and Day 21 (Fig. 2I). Consistent with the activation of the tendon
185 program, 3D-hASC constructs did not express osteogenic or adipogenic markers and did not
186 contain any adipocytes or osteocytes (Supplementary Fig. 3B-D). It has to be noted that hASCs
187 displayed the ability to differentiate into adipocytes and osteocytes in appropriate culture media
188 in 2D-culture conditions (Supplementary Fig. 3A-C) [47,50]. The cartilage-specific collagen
189 gene *COL2A1* was not detected 3D-hASC constructs (Fig. 2J), indicating that hASCs had not
190 differentiated into cartilage cells.
191 We conclude that hASCs undergo towards a tendon program when cultured in 3D-
192 conditions in a collagen gel maintained between two anchor points.
193
194 *The Young's modulus of 3D-hASC constructs increases over time.*
195 In order to assess whether the activation of the tendon program in hASCs was correlated with
196 a stiffening of the 3D-constructs, we measured the Young's modulus of 3D-hASC constructs
197 in the course of the 21 Days of culture. We used nanoindentation [51] to probe the mechanical
198 properties of the 3D-hASC constructs at the local scale (micron scale), with the application of
199 controlled deformations on the surface of the sample. To maintain the 3D-hASC constructs in
200 an immobile position during the nanoindentation experiments, they were detached from their
201 anchor points and deposited onto a support composed of grooves whose length and diameters
202 were adjusted according to constructs geometry. The support was maintained in a petri dish
203 with agarose gel, while 3D-hASC constructs were fixed to the support using dissection pins
204 inserted through the anchor stems and in the agarose gel (Fig. 3A). Indentation was performed
205 by moving the base of the cantilever at a constant speed of $10\mu m.s^{-1}$, with beads of diameters
206 ranged from 50 to 100 µm (Fig. 3B-D). The relationship between applied force and deformation
207 provides information about 3D-hASCs construct mechanical properties. In particular, tissue
208 effective Young's modulus E_{eff} was calculated by fitting the force-indentation curve over a one-
209 micron indentation range using the Hertz model (Fig. 3E, see methods). The effective Young's
210 modulus increased significantly during the 21 Days of construct culture starting from 1.3 kPa
211 at Day 0 to 9.2 kPa at Day 21 (Fig. 3F). Notably, E_{eff} increased by two-fold factor every seven
212 days. The effective Young's modulus of 3D-no cell constructs not seeded with cells remains
213 constant for 21 days, at 0.4 kPa (Fig. 3F).
214 We conclude that 3D-hASC constructs display an increased stiffness over time.

215

216 *Extracellular matrix gene expression is correlated with changes in viscoelastic properties of*
217 *3D-hASC constructs.*

218 Tendon stiffness relies on the synthesis of a dense and organized extracellular matrix generated
219 by tendon cells. We thus analysed the expression of transcripts encoding tendon-associated
220 collagens and fibrillogenesis-associated proteins during 3D-hASC constructs formation.
221 Similarly to *COL1A1* (Fig. 1G), the mRNA levels of the tendon-associated collagens *COL6A3*
222 and *COL14A1* were detected at Day 0, increased until Day 7 and remained higher at Day 21
223 compared to Day 0 (Fig. 4A-B). We also analysed the expression of genes encoding
224 fibrillogenesis-associated proteins, *DPT*, *DCN*, *POSTN* and *LOX* which exhibit an elevated
225 enrichment score in E14.5 compared to E11.5 *SCX*-positive cells during mouse limb
226 development [52]. The transcript levels of *DPT*, *DCN*, *POSTN* and *LOX* were significantly
227 increased during human 3D-hASC construct formation (Fig. 4C-F). The persistent increase of
228 tendon collagen and collagen fibrillogenesis gene expression was indicative of matrix
229 production and parallel the increase of effective Young's modulus (Fig. 3F) during 3D-hASCs
230 construct formation. In addition, the increased expression of *DPT*, *DCN*, *POSTN*, *THBS2* and
231 *LOX*, regulators of ECM network, also suggested that the structure and organisation of the ECM
232 was modified during the course of 3D-hASC construct formation. We thus tested whether ECM
233 transcript expression was accompanied with a modification of the viscoelastic properties of 3D-
234 hASC constructs along time. To do this, we carried out stress relaxation experiments using
235 nanoindentation (Fig. 5). In particular, we calculated the percentage of relaxation r_{relax} from the
236 peak force F_{max} measured at the end of the indentation ramp and the force $F_{t=10s}$ measured after
237 10 seconds of relaxation ($r_{relax} = (F_{max}-F_{t=10s})/F_{max}$). The higher this ratio is, the more liquid-like
238 the material. Oppositely, a smaller ratio indicates more solid, elastic-like viscoelastic properties.
239 On Day 0, the percentage of relaxation of 3D-hASCs was 35% and decreased along time down
240 to 24% on Day 21 (Fig. 5E), in parallel with the increase of ECM transcript levels. Interestingly,
241 the percentage of relaxation of 3D-no cell constructs on Day 0 was 23%, decreased to 15% on
242 Day 7 and remained constant (Fig. 5E).

243 We conclude that the 3D-hASC constructs acquire solid-like properties, consistent with
244 the expression of ECM transcripts during the time course of the cultures.

245

246 *3D-hASC constructs organize into two cell populations.*

247 In order to analyse cell organisation, we performed longitudinal and transverse sections of 3D-
248 hASC constructs (Fig. 1E, Supplementary Fig. 4, Fig. 6). We identified two cell populations,

249 one at the centre and the other one at the periphery as a ring, as soon as Day 2 (Fig. 6B).
250 Phalloidin staining showed that the peripheral cell population formed a ring composed of 3 to
251 4 cell layers from Day 4 to Day 21, which was separated from the central region by a sharp
252 interface (Fig. 6B). Cell density at the ring and the centre was maintained from Day 4 to Day
253 21 (Fig. 6C). Interestingly, the expression of ECM genes evolved in the two cell populations in
254 a different manner (Fig. 1I, 2F). *COL1A1* was expressed in both centre and ring cells of 3D-
255 hASC constructs with in situ hybridization from Day 7 to Day 14 (Fig. 1I). However, at Day
256 21, *COL1A1* displayed stronger expression in centre cells compared to ring cells (Fig. 1I). By
257 contrast, *THBS2* was visualized in both centre and ring 3D-hASCs construct cells along the 21
258 days of culture (Fig. 2F). In addition, a marker of peripheral cells of adult rat tendons *COL3A1*
259 [53] was detected both in centre and ring cells of 3D-hASC constructs, suggesting that the cells
260 at the periphery were not mature peritenon cells (Supplementary Fig. 5).
261 We conclude that 3D-hASC constructs self-organize into cell populations with different
262 location.
263
264 **Discussion**
265
266 This study showed that hASCs embedded into a cylindrical scaffold of type I-collagen attached
267 to two anchor points leads to the expression of transcription factors and matrisome genes
268 specific of tendon phenotype, and to the acquisition of viscoelastic properties reminiscent of
269 tendon embryonic development.
270
271 *Molecular progression of the tendon phenotype in hASCs in 3D-cultures*
272 With no external molecular cues other than the culture medium, hASCs mixed in a 3D-collagen
273 gel expressed tendon genes encoding transcription factors regulating *COL1A1* transcription and
274 tendon matrix genes. The molecular progression in 3D-hASCs is reminiscent of tendon gene
275 expression during development. The transcriptional regulators of *COL1A1* transcription, *SCX*
276 and *MKX* are sequentially expressed during 3D-hASC constructs formation, as during mouse
277 tendon development [8,9]. The expression pattern of *SCX* displays a bell shape, while the
278 tendon matrix gene expression increases overtime in 3D-hASC constructs, consistent with SCX
279 function as a starter of the developmental tendon program. The sequential expression of *SCX*
280 and *TNMD* and the decrease of *SCX* and *TNMD* at Day 21 in the 3D-hASC constructs are
281 consistent with *TNMD* regulation by SCX [6,11]. The two newly-identified genes, *TM4SF1* and
282 *ANXA1,* coding for a Tetraspanin transmembrane protein and AnnexinA1, respectively, display

283 a regular increase overtime as the *LOX* gene (lysyl oxidase proteins). Interestingly, the *TM4SF1*,
284 *ANXA1* and *LOX* genes have been identified in a fibroblast cluster for good prognosis in bladder
285 cancer [54] and are seen as therapeutic targets for fibrosis [55–57]. ANXA1 and S100A10
286 belong to two families of proteins known to form hetero-tetramers [58], suggesting that ANXA1
287 interacts with S100A10 to maintain the tendon phenotype of 3D-hASC constructs. The mRNA
288 expression levels of the tendon-associated collagen genes (*COL1A1*, *COL6A3*, *COL14A1)* and
289 genes encoding proteins involved in tendon collagen fibrillogenesis (*THBS2*, *DCN, POSTN,*
290 *DPT)* rise sharply during the formation of 3D-hASC constructs, and were maintained at high
291 levels at the end of culture. These results indicate that the reduced expression of *SCX* in 3D-
292 hASCs does not affect the molecular identity of tendon ECM in the constructs.
293 Our study shows that 3D-hASCs activate the tendon differentiation program, without
294 dynamic mechanical stimulation or molecule addition, mimicking the development of
295 embryonic tendons.
296
297 *Progression of mechanical properties of hASCs in 3D-cultures*
298 During the 21-day culture period, the 3D-hASCs showed reduced diameter, increased stiffness
299 and reduced relaxation. The reduction in the diameter of 3D-hASC constructs was already
300 observed in 3D-constructs using human dermal fibroblasts (HDF01035) or calf patellar tendon
301 cells embedded in a collagen gel [59,60]. Because the diameters of 3D-no cell constructs
302 without any cell remained constant, we conclude that hASCs were responsible for the collagen
303 compaction of 3D-hASC constructs.
304 There is a linear increase of the stiffness of 3D-hASC constructs during the time of
305 culture. Notably, E_{eff} increased by two-fold factor every seven days. This indicates that this
306 long time-scale stiffening is unlikely to be due to ECM compaction, which occurred almost
307 exclusively during the first week of culture. We rather believe that the expression of genes
308 encoding specific ECM components would drive collagen compaction. After three weeks of
309 cell culture, 3D-hASC constructs exhibited a Young's modulus values comprised between 5.6
310 and 18.3 kPa. Interestingly, measurements of nanoscale elastic modulus of chicken embryonic
311 calcaneus tendons calculated similarly through Hertz contact theory gave results of same order
312 of magnitude (5-17 kPa) [2,61]. This suggests that 3D-hASC constructs mimic the progression
313 of mechanical properties observed during embryonic tendon development. In studies using
314 human adult tendon fibroblasts (not MSCs) to generate 3D constructs, Young's modulus
315 measurements lead to a value close to that found by tensile tests in adult tendons, of the order
316 of MPa [32,35].

317

318 *Link between the progression of ECM expression and mechanics in 3D-hASC constructs*

319 The increase of expression of ECM-encoding genes parallels the stiffness increase and
320 concomitant relaxation reduction of 3D-hASC constructs. We see this correlation as a
321 bidirectional interaction between mechanical properties and ECM components during the time
322 of the culture. It is recognized that changes of physical properties act on ECM composition and
323 conversely, ECM interferes with mechanical properties [62]. We found that hASCs
324 progressively acquired a spindle-shaped form associated with elongation of the cell shape
325 during the course of the 3D-culture, as observed in native tendons. The elongated shape of cells
326 observed in native tendons and 3D-hASC constructs is probably involved in tendon matrix
327 production, since nuclear response upon deformation is recognized to include changes in
328 transcriptional activity [63].

329 3D-hASC constructs self-organize into two cell populations, one being at the centre of
330 the construct and the other forming a ring at the periphery. Such organisation has been
331 previously described in 3D-constructs generated with the Flexcell technology either with
332 hASCs [30] or avian tendon internal fibroblasts [64]. This cell organisation could be an effect
333 of the geometry of the constructions defined by the anchoring points, which may orient cell
334 shape and ECM. The peripheral cells layer of 3D-hASC constructs is reminiscent of peritenon
335 surrounding native tendon. This is consistent with the lower *COL1A1* expression in the ring
336 cells compared to centre cells in 3D-hASC constructs at Day 21 (Fig. 1I) observed in equine
337 and rat peritenon cells versus tendon core cells [53,65]. *COL3A1* was identified recently as a
338 peritenon marker in adult rat patellar tendons [53]. However, *COL3A1* was detected both at the
339 centre and the periphery of 3D-hASC constructs (Supplementary Fig. 5), indicating that
340 *COL31A1* expression does not discriminate the peritenon identity between ring and center cells
341 in 3D-hASC constructs. Interestingly, a peripheral layer has been identified surrounding
342 developing tendons in mouse and chicken embryos [4,15,66], indicating that future peritenon
343 cells are present early during the tendon program.

344 Although the 3D-hASC constructs display a tendon matrisome gene expression profile
345 at 3 weeks, we do not exclude that external mechanical cues would improve the tendon
346 phenotype of 3D-hASC constructs as already reported [45,67]. During development, muscle
347 contractions are recognized to maintain *SCX* expression and the tendon phenotype in
348 developing tendons [26]. An interesting hypothesis is that application of external mechanical
349 cues would prevent *SCX* and *TNDM* down-regulation in 21-day-old 3D-hASC constructs.

350

351 In summary, we have established that hASCs, cultured in 3D-system with minimal molecular
352 and mechanical cues, progress into the tendon differentiation program along three weeks of
353 culture. The molecular tendon program is associated with variations of mechanical properties
354 reminiscent of embryonic tendon development.
355
356 **Experimental procedures**
357
358 *Cell sample collection*
359 Human abdominal subcutaneous adipose tissues were obtained from healthy donors after
360 liposuction surgery (AP-HP Saint-Antoine Hospital, Paris, France). Human Adipose stromal
361 cells (hASCs) were isolated from 3 healthy donors (one woman and two men).
362 All donors provided their written, informed consent to the use of their tissue specimens for
363 research purposes. The study was performed in compliance with the principles of the
364 Declaration of Helsinki and was approved by an institutional review board. The study was
365 approved by the French regulatory authorities (Codecoh DC2023-5617). Cells were
366 cryopreserved in 2mL cryotubes (2x106 cells per vial) stored in liquid nitrogen tanks.
367
368 *Cell amplification*
369 For each experiments, cell vials were thawed 2-3 min in a 37°C water bath and transferred in
370 T25 cell culture flasks (Gibco) with 5ml of hASCs culture medium containing Minimum
371 Essential Mediun (αMEM; Gibco; ref 22571-020) complemented with 10% Fetal Calf Serum
372 (FCS; Gibco; ref 35-079-CV), 1% HEPES (1M, sigma; ref H0887-100ml), 1% glutamine
373 (100X, 200mM, Gibco; ref 25030-024), 1% Penicillin/Streptomycin (Gibco; ref 15140-122)
374 and 2.5 ng/mL FGF2 (PeproTech, Rocky Hill, NJ; ref 100-18B). Confluent cells were submitted
375 to 2 passages, at 1:9 and 1:3 ratio. For each passage, we used 0.05% Trypsin (Gibco; ref 25300-
376 054) for 5 minutes.
377
378 *Preparation of 3D-hASC constructs*
379 3D-hASC constructs were prepared as described [42]. Briefly, sub confluent cells were
380 detached in 5 ml of 0.05% trypsin for 5 minutes, then suspended with hASC culture medium
381 (described below) and counted with a Malassez counting chamber. 16.2 million cells (600,000
382 cells per 3D-hASC construct) were centrifuged at 1200 rpm for 5 minutes and resuspended in
383 4.05 mL of Type I collagen solution containing 70% Purecoll (Sigma-Aldritch, Oakville,
384 Canada; ref 5074-35ml), 10% FCS and 20% αMEM brought to 7.4 pH with 0.1 N NaOH

385 immediately before use. 150 µl of hASCs-collagen mix was pipetted into each well of an
386 untreated TissueTrain© plate (FlexCell International, Hillsborough NC; ref TTLC-4001C)
387 according to the manufacturer's instructions. The collagen hydrogel was allowed to set for 2
388 hours, and the 3D-hASC constructs were covered with 2 ml of hASC culture medium completed
389 with 0.25 mM ascorbic acid. The medium was replaced every 2-3 Days.
390 *3D-hASC construct sections*
391 3D-hASC constructs were fixed in 1% paraformaldehyde (PFA, Gibco Sigma; ref 158127-
392 100G) overnight at 4°C, washed in 1X PBS (Gibco; ref :14190-094) and put in a 15% sucrose
393 solution at 4°C for 3 Days. Before inclusion, 3D-hASC constructs were incubated in a 7,5%
394 gelatin-15% sucrose solution in a 37°C water bath for 1 hour. Included 3D-hASC constructs
395 were then frozen at -80°C in isopentane for 1 minute and 12µm longitudinal and transversal
396 cryosections were generated with a CM3050 S Cryostat (Leica Biosystems).
397
398 *Cell angle measurements*
399 Longitudinal sections were stained with DAPI (D9542, Sigma-Aldrich) to visualize cell nuclei
400 and phalloidin (A12380 Alexa Fluor Phalloidin, Invitrogen/ ThermoFisher scientific) to
401 visualize cytoskeletal F-actin. Fluorescent images were captured using a Zeiss Axio Observer
402 Z1 microscope equipped with a Zeiss Apotome 2 and an Axiocam 506 monochrome camera.
403 Cell/nucleus angles relative to the axis of the 3D-hASC constructs were measured using Fiji
404 Image J software.
405
406 *RNA isolation*
407 Entire 3D-hASC constructs were put in 500µL RLT (Qiagen; ref 74106) and homogenized
408 using a mechanical disruption device (Lysing Matrix A, Fast Prep MP1, 4 × 30 s, 6 $m.s^{-1}$). Total
409 RNA was isolated using the RNeasy mini kit (Qiagen; ref 74106), according to the
410 manufacturer's instructions, including a 15 min of DNase I (Qiagen; ref 79254) treatment.
411
412 *Reverse-Transcription and quantitative real time PCR*
413 500ng of total RNAs extracted from each 3D-hASCs construct, for each timepoint, were
414 Reverse Transcribed using the High Capacity Retro-transcription kit (Applied Biosystems; ref
415 4387406). Quantitative PCR analyses were performed using primers listed in Supplementary
416 Table 1 and SYBR Green PCR Master Mix (Applied Biosystems; ref 4385614). The relative
417 mRNA levels were calculated using the $2^{-\Delta\Delta Ct}$ method [68]. The cycle threshold (C_T)
418 corresponds to the number of cycles required for the fluorescent signal to cross the threshold

(to exceed background level). The ΔC_Ts were obtained from C_T normalized to *YWHAZ* C_T level in each sample. The primers used for RT-qPCR experiments are listed in Supplementary table 1.

In situ hybridization

3D-hASCs construct 12µm cryosections were subject to a standard in situ hybridization protocol [69]. *COL1A1, SCX, THBS2 and COL3A1* and probes were generated using a Roboprobe kit (Promega; ref P1460), according to manufacturer's instructions. Images were captured using a Nanozoomer SQ Digital Slide Scanner with NDP.view2 software (Hamamatsu Photonics). The primers used for probe synthesis are listed in Supplementary table 1.

Nanoindentation measurements

Live 3D-hASC constructs were detached from their anchor points and immediately fixed onto a 3D-printed support. To avoid sliding of the construct during mechanical testing, the support was designed with three half-cylindrical grooves at its surface whose diameters were adjusted to the typical 3D-hASC constructs diameters. In order to conserve the original length of the 3D-hASCs construct, the length of the support was also calibrated to the original distance between the anchor points in the bioreactor. The support was then embedded in an agarose gel in a Petri dish, and the samples were immersed in culture medium. Mechanical testing was performed at room temperature, using a Piuma nano-indenter (Optics11 Life), as described in the main text. Samples were positioned under the probe using a magnifying glass. Five measurements were performed along the 3D-hASCs construct length and their mean value was calculated to extract effective Young's modulus and percentage of stress relaxation for each sample.

The effective Young's modulus E_{eff} was calculated from a fit of the force versus indentation curve over a 1µm indentation course and using a Hertzian contact model as follows:

$$F = \frac{4}{3} E_{eff} \sqrt{R_i} \cdot h^{3/2}$$

where F is the force, Ri the tip radius, and h the indentation.

Statistical analyses

Data was analysed using the non-parametric Mann-Whitney test with Graphpad Prism V10. Results are shown as means ± standard deviations. The p-values are indicated either with the value or with * or #.

Funding sources

This work was supported by the CNRS, INSERM, Sorbonne University and ANR_TENORS.

Acknowledgements

We would like to thank Mathieu Hautefeuille for proofreading the manuscript.

References

[1] J. Peltonen, N.J. Cronin, L. Stenroth, T. Finni, J. Avela, Viscoelastic properties of the achilles tendon in vivo, Springerplus 2 (2013) 1–8. https://doi.org/10.1186/2193-1801-2-212.

[2] B.K. Connizzo, A.J. Grodzinsky, Tendon exhibits complex poroelastic behavior at the nanoscale as revealed by high-frequency AFM-based rheology, J Biomech 54 (2017) 11–18. https://doi.org/10.1016/j.jbiomech.2017.01.029.

[3] A.H. Huang, J.L. Galloway, Current and emerging technologies for defining and validating tendon cell fate, Journal of Orthopaedic Research 41 (2023) 2082–2092. https://doi.org/10.1002/jor.25632.

[4] E. Hirsinger, C. Blavet, M.A. Bonnin, L. Bellenger, T. Gharsalli, D. Duprez, Limb connective tissue is organized in a continuum of promiscuous fibroblast identities during development, IScience 27 (2024). https://doi.org/10.1016/j.isci.2024.110305.

[5] R. Schweitzer, J.H. Chyung, L.C. Murtaugh, A.E. Brent, V. Rosen, E.N. Olson, A. Lassar, C.J. Tabin, Analysis of the tendon cell fate using Scleraxis, a specific marker for tendons and ligaments, Development 128 (2001) 3855–3866. https://doi.org/10.1242/dev.128.19.3855.

[6] N.D. Murchison, B.A. Price, D.A. Conner, D.R. Keene, E.N. Olson, C.J. Tabin, R. Schweitzer, Regulation of tendon differentiation by scleraxis distinguishes force-transmitting tendons from muscle-anchoring tendons, Development 134 (2007) 2697 LP – 2708. https://doi.org/10.1242/dev.001933.

[7] M.-J. Guerquin, B. Charvet, G. Nourissat, E. Havis, O. Ronsin, M.-A. Bonnin, M. Ruggiu, I. Olivera-Martinez, N. Robert, Y. Lu, K.E. Kadler, T. Baumberger, L. Doursounian, F. Berenbaum, D. Duprez, Transcription factor EGR1 directs tendon differentiation and promotes tendon repair, Journal of Clinical Investigation 123 (2013). https://doi.org/10.1172/JCI67521.

[8] Y. Ito, N. Toriuchi, T. Yoshitaka, H. Ueno-Kudoh, T. Sato, S. Yokoyama, K. Nishida, T. Akimoto, M. Takahashi, S. Miyaki, H. Asahara, The Mohawk homeobox gene is a critical regulator of tendon differentiation, Proc Natl Acad Sci U S A 107 (2010) 10538–10542. https://doi.org/10.1073/pnas.1000525107.

[9] W. Liu, S.S. Watson, Y. Lan, D.R. Keene, C.E. Ovitt, H. Liu, R. Schweitzer, R. Jiang, The Atypical Homeodomain Transcription Factor Mohawk Controls Tendon Morphogenesis, Mol Cell Biol 30 (2010) 4797–4807. https://doi.org/10.1128/mcb.00207-10.

[10] C. Shukunami, A. Takimoto, M. Oro, Y. Hiraki, Scleraxis positively regulates the expression of tenomodulin, a differentiation marker of tenocytes, Dev Biol 298 (2006) 234–247. https://doi.org/10.1016/j.ydbio.2006.06.036.

[11] C. Shukunami, A. Takimoto, Y. Nishizaki, Y. Yoshimoto, S. Tanaka, S. Miura, H. Watanabe, T. Sakuma, T. Yamamoto, G. Kondoh, Y. Hiraki, Scleraxis is a transcriptional activator that regulates the expression of Tenomodulin, a marker of

498 mature tenocytes and ligamentocytes, Sci Rep 8 (2018) 3155.
499 https://doi.org/10.1038/s41598-018-21194-3.
500 [12] D. Docheva, E.B. Hunziker, R. Fässler, O. Brandau, Tenomodulin is necessary for
501 tenocyte proliferation and tendon maturation, Mol Cell Biol 25 (2005) 699–705.
502 https://doi.org/10.1128/MCB.25.2.699-705.2005.
503 [13] S. Dex, P. Alberton, L. Willkomm, T. Söllradl, S. Bago, S. Milz, M. Shakibaei, A.
504 Ignatius, W. Bloch, H. Clausen-Schaumann, C. Shukunami, M. Schieker, D. Docheva,
505 Tenomodulin is Required for Tendon Endurance Running and Collagen I Fibril
506 Adaptation to Mechanical Load, EBioMedicine 20 (2017) 240–254.
507 https://doi.org/10.1016/j.ebiom.2017.05.003.
508 [14] A.H. Huang, S.S. Watson, L. Wang, B.M. Baker, H. Akiyama, J. V Brigande, R.
509 Schweitzer, Requirement for scleraxis in the recruitment of mesenchymal progenitors
510 during embryonic tendon elongation, Development 146 (2019) dev182782.
511 https://doi.org/10.1242/dev.182782.
512 [15] E. Havis, M.-A. Bonnin, I. Olivera-Martinez, N. Nazaret, M. Ruggiu, J. Weibel, C.
513 Durand, M.-J. Guerquin, C. Bonod-Bidaud, F. Ruggiero, R. Schweitzer, D. Duprez,
514 Transcriptomic analysis of mouse limb tendon cells during development, Development
515 141 (2014) 3683–3696. https://doi.org/10.1242/dev.108654.
516 [16] T.R. Kyriakides, Y.H. Zhu, L.T. Smith, S.D. Bain, Z. Yang, M.T. Lin, K.G. Danielson,
517 R. V. Iozzo, M. LaMarca, C.E. McKinney, E.I. Ginns, P. Bornstein, Mice that lack
518 thrombospondin 2 display connective tissue abnormalities that are associated with
519 disordered collagen fibrillogenesis, an increased vascular density, and a bleeding
520 diathesis, Journal of Cell Biology 140 (1998) 419–430.
521 https://doi.org/10.1083/jcb.140.2.419.
522 [17] T.C. Pan, R.Z. Zhang, D. Markova, M. Arita, Y. Zhang, S. Bogdanovich, T.S.
523 Khurana, C.G. Bönnemann, D.E. Birk, M.L. Chu, COL6A3 protein deficiency in mice
524 leads to muscle and tendon defects similar to human collagen VI congenital muscular
525 dystrophy, Journal of Biological Chemistry 288 (2013) 14320–14331.
526 https://doi.org/10.1074/jbc.M112.433078.
527 [18] H.L. Ansorge, X. Meng, G. Zhang, G. Veit, M. Sun, J.F. Klement, D.P. Beason, L.J.
528 Soslowsky, M. Koch, D.E. Birk, Type XIV collagen regulates fibrillogenesis:
529 Premature collagen fibril growth and tissue dysfunction in null mice, Journal of
530 Biological Chemistry 284 (2009) 8427–8438. https://doi.org/10.1074/jbc.M805582200.
531 [19] G. Zhang, Y. Ezura, I. Chervoneva, P.S. Robinson, D.P. Beason, E.T. Carine, L.J.
532 Soslowsky, R. V. Iozzo, D.E. Birk, Decorin regulates assembly of collagen fibrils and
533 acquisition of biomechanical properties during tendon development, J Cell Biochem 98
534 (2006) 1436–1449. https://doi.org/10.1002/jcb.20776.
535 [20] J.E. Ackerman, S.N. Muscat, E. Adjei-Sowah, A. Korcari, A.E.C. Nichols, M.R.
536 Buckley, A.E. Loiselle, Identification of Periostin as a critical niche for myofibroblast
537 dynamics and fibrosis during tendon healing, Matrix Biology 125 (2024) 59–72.
538 https://doi.org/10.1016/j.matbio.2023.12.004.
539 [21] H. Li, A. Korcari, D. Ciufo, C.L. Mendias, S.A. Rodeo, M.R. Buckley, A.E. Loiselle,
540 G.S. Pitt, C. Cao, Increased Ca2+ signaling through CaV 1.2 induces tendon
541 hypertrophy with increased collagen fibrillogenesis and biomechanical properties,
542 FASEB J 37 (2023) e23007. https://doi.org/10.1096/fj.202300607R.
543 [22] O. Okamoto, S. Fujiwara, Dermatopontin, a Novel Player in the Biology of the
544 Extracellular Matrix, Connect Tissue Res 47 (2006) 177–189.
545 https://doi.org/10.1080/03008200600846564.
546 [23] A.J. de Micheli, J.B. Swanson, N.P. Disser, L.M. Martinez, N.R. Walker, D.J. Oliver,
547 B.D. Cosgrove, C.L. Mendias, Single-cell transcriptomic analysis identifies extensive

heterogeneity in the cellular composition of mouse Achilles tendons, Am J Physiol Cell Physiol 319 (2020) C885–C894. https://doi.org/10.1152/ajpcell.00372.2020.

[24] T. Omoto, D. Yimiti, Y. Sanada, M. Toriyama, C. Ding, Y. Hayashi, Y. Ikuta, T. Nakasa, M. Ishikawa, M. Sano, M. Lee, T. Akimoto, C. Shukunami, S. Miyaki, N. Adachi, Tendon-Specific Dicer Deficient Mice Exhibit Hypoplastic Tendon Through the Downregulation of Tendon-Related Genes and MicroRNAs, Front Cell Dev Biol 10 (2022) 1–14. https://doi.org/10.3389/fcell.2022.898428.

[25] P.K. Nguyen, K. Hall, I. Holt, C.K. Kuo, Recombinant lysyl oxidase effects on embryonic tendon cell phenotype and behavior, Journal of Orthopaedic Research 41 (2023) 2175–2185. https://doi.org/10.1002/jor.25655.

[26] L. Gaut, D. Duprez, Tendon development and diseases, Wiley Interdiscip Rev Dev Biol 5 (2016) 5–23. https://doi.org/10.1002/wdev.201.

[27] E. Havis, M.-A. Bonnin, J. Esteves de Lima, B. Charvet, C. Milet, D. Duprez, TGFβ and FGF promote tendon progenitor fate and act downstream of muscle contraction to regulate tendon differentiation during chick limb development, Development 143 (2016) 3839–3851. https://doi.org/10.1242/dev.136242.

[28] K. Otabe, H. Nakahara, A. Hasegawa, T. Matsukawa, F. Ayabe, N. Onizuka, M. Inui, S. Takada, Y. Ito, I. Sekiya, T. Muneta, M. Lotz, H. Asahara, Transcription factor mohawk controls tenogenic differentiation of bone marrow mesenchymal stem cells in vitro and in vivo, Journal of Orthopaedic Research 33 (2015) 1–8. https://doi.org/10.1002/jor.22750.

[29] L. Gaut, M.A. Bonnin, C. Blavet, I. Cacciapuoti, M. Orpel, M. Mericskay, D. Duprez, Mechanical and molecular parameters that influence the tendon differentiation potential of C3H10T1/2 cells in 2D- And 3D-culture systems, Biol Open 9 (2020). https://doi.org/10.1242/bio.047928.

[30] G. Yang, B.B. Rothrauff, H. Lin, R. Gottardi, P.G. Alexander, R.S. Tuan, Enhancement of tenogenic differentiation of human adipose stem cells by tendon-derived extracellular matrix, Biomaterials 34 (2013) 9295–9306. https://doi.org/10.1016/j.biomaterials.2013.08.054.

[31] D. Jaiswal, L. Yousman, M. Neary, E. Fernschild, B. Zolnoski, S. Katebifar, S. Rudraiah, A.D. Mazzocca, S.G. Kumbar, Tendon tissue engineering: Biomechanical considerations, Biomedical Materials (Bristol) 15 (2020). https://doi.org/10.1088/1748-605X/ab852f.

[32] A. Herchenhan, M.L. Bayer, R.B. Svensson, S.P. Magnusson, M. Kjær, In vitro tendon tissue development from human fibroblasts demonstrates collagen fibril diameter growth associated with a rise in mechanical strength, Developmental Dynamics 242 (2013) 2–8. https://doi.org/10.1002/dvdy.23896.

[33] A. Herchenhan, F. Uhlenbrock, P. Eliasson, M. Weis, D. Eyre, K.E. Kadler, S.P. Magnusson, M. Kjaer, Lysyl oxidase activity is required for ordered collagen fibrillogenesis by tendon cells, Journal of Biological Chemistry 290 (2015) 16440–16450. https://doi.org/10.1074/jbc.M115.641670.

[34] Z. Kapacee, S.H. Richardson, Y. Lu, T. Starborg, D.F. Holmes, K. Baar, K.E. Kadler, Tension is required for fibripositor formation, Matrix Biology 27 (2008) 371–375. https://doi.org/10.1016/j.matbio.2007.11.006.

[35] A.M. Avey, O. Valdez, K. Baar, Characterization of an in vitro engineered ligament model, Matrix Biol Plus 21 (2024). https://doi.org/10.1016/j.mbplus.2023.100140.

[36] M.L. Bayer, C.Y.C. Yeung, K.E. Kadler, K. Qvortrup, K. Baar, R.B. Svensson, S. Peter Magnusson, M. Krogsgaard, M. Koch, M. Kjaer, The initiation of embryonic-like collagen fibrillogenesis by adult human tendon fibroblasts when cultured under tension, Biomaterials 31 (2010) 4889–4897. https://doi.org/10.1016/j.biomaterials.2010.02.062.

[37] N.S. Kalson, D.F. Holmes, Z. Kapacee, I. Otermin, Y. Lu, R.A. Ennos, E.G. Canty-Laird, K.E. Kadler, An experimental model for studying the biomechanics of embryonic tendon: Evidence that the development of mechanical properties depends on the actinomyosin machinery, Matrix Biology 29 (2010) 678–689. https://doi.org/10.1016/j.matbio.2010.08.009.

[38] C.Y.C. Yeung, L.A.H. Zeef, C. Lallyett, Y. Lu, E.G. Canty-Laird, K.E. Kadler, Chick tendon fibroblast transcriptome and shape depend on whether the cell has made its own collagen matrix, Sci Rep 5 (2015). https://doi.org/10.1038/srep13555.

[39] C.F. Hsieh, Z. Yan, R.G. Schumann, S. Milz, C.G. Pfeifer, M. Schieker, D. Docheva, In vitro comparison of 2D-cell culture and 3D-cell sheets of scleraxis-programmed bone marrow derived mesenchymal stem cells to primary tendon stem/progenitor cells for tendon repair, Int J Mol Sci 19 (2018). https://doi.org/10.3390/ijms19082272.

[40] Z. Kapacee, C.Y.C. Yeung, Y. Lu, D. Crabtree, D.F. Holmes, K.E. Kadler, Synthesis of embryonic tendon-like tissue by human marrow stromal/mesenchymal stem cells requires a three-dimensional environment and transforming growth factor β3, Matrix Biology 29 (2010) 668–677. https://doi.org/10.1016/j.matbio.2010.08.005.

[41] L. Gaut, N. Robert, A. Delalande, M.A. Bonnin, C. Pichon, D. Duprez, EGR1 regulates transcription downstream of mechanical signals during tendon formation and healing, PLoS One 11 (2016) 1–16. https://doi.org/10.1371/journal.pone.0166237.

[42] A. Scott, P. Danielson, T. Abraham, G. Fong, A. V. Sampaio, T.M. Underhill, Mechanical force modulates scleraxis expression in bioartificial tendons, Journal of Musculoskeletal Neuronal Interactions 11 (2011) 124–132.

[43] S. Pentzold, B. Wildemann, Mechanical overload decreases tenogenic differentiation compared to physiological load in bioartificial tendons, J Biol Eng 16 (2022) 1–10. https://doi.org/10.1186/s13036-022-00283-y.

[44] C.K. Kuo, R.S. Tuan, Mechanoactive tenogenic differentiation of human mesenchymal stem cells, Tissue Eng Part A 14 (2008) 1615–1627. https://doi.org/10.1089/ten.tea.2006.0415.

[45] H. Park, S.N. Nazhat, D.H. Rosenzweig, Mechanical activation drives tenogenic differentiation of human mesenchymal stem cells in aligned dense collagen hydrogels, Biomaterials 286 (2022) 121606. https://doi.org/10.1016/j.biomaterials.2022.121606.

[46] P. Zuk, Adipose-Derived Stem Cells in Tissue Regeneration: A Review, Int Sch Res Notices 2013 (2013) e713959. https://doi.org/10.1155/2013/713959.

[47] L.E. Kokai, K. Marra, J.P. Rubin, Adipose stem cells: Biology and clinical applications for tissue repair and regeneration, Translational Research 163 (2014) 399–408. https://doi.org/10.1016/j.trsl.2013.11.009.

[48] V. Béréziat, C. Mazurier, M. Auclair, N. Ferrand, S. Jolly, T. Marie, L. Kobari, I. Toillon, F. Delhommeau, B. Fève, A.K. Larsen, M. Sabbah, L. Garderet, Systemic dysfunction of osteoblast differentiation in adipose-derived stem cells from patients with multiple myeloma, Cells 8 (2019) 1–16. https://doi.org/10.3390/cells8050441.

[49] J. Gorwood, T. Ejlalmanesh, C. Bourgeois, M. Mantecon, C. Rose, M. Atlan, D. Desjardins, R. Le Grand, B. Fève, O. Lambotte, J. Capeau, V. Béréziat, C. Lagathu, SIV Infection and the HIV Proteins Tat and Nef Induce Senescence in Adipose Tissue and Human Adipose Stem Cells, Resulting in Adipocyte Dysfunction, Cells 9 (2020). https://doi.org/10.3390/cells9040854.

[50] M. Waldner, W. Zhang, I.B. James, K. Allbright, E. Havis, J.M. Bliley, A. Almadori, R. Schweizer, J.A. Plock, K.M. Washington, V.S. Gorantla, M.G. Solari, K.G. Marra, J.P. Rubin, Characteristics and immunomodulating functions of adipose-derived and bone marrow-derived mesenchymal stem cells across defined human leukocyte antigen barriers, Front Immunol 9 (2018). https://doi.org/10.3389/fimmu.2018.01642.

[51] H. Van Hoorn, N.A. Kurniawan, G.H. Koenderink, D. Iannuzzi, Local dynamic mechanical analysis for heterogeneous soft matter using ferrule-top indentation, Soft Matter 12 (2016) 3066–3073. https://doi.org/10.1039/c6sm00300a.
[52] E. Havis, M.-A. Bonnin, I. Olivera-Martinez, N. Nazaret, M. Ruggiu, J. Weibel, C. Durand, M.-J. Guerquin, C. Bonod-Bidaud, F. Ruggiero, R. Schweitzer, D. Duprez, Transcriptomic analysis of mouse limb tendon cells during development, Development (Cambridge) 141 (2014). https://doi.org/10.1242/dev.108654.
[53] D. Steffen, M. Mienaltowski, K. Baar, Spatial gene expression in the adult rat patellar tendon, Matrix Biol Plus 19–20 (2023). https://doi.org/10.1016/j.mbplus.2023.100138.
[54] J. Wang, Z. Tan, Y. Huang, C. Li, P. Zhan, H. Wang, H. Li, Integrating single-cell RNA-seq to identify fibroblast-based molecular subtypes for predicting prognosis and therapeutic response in bladder cancer, 2024. www.aging-us.comwww.aging-us.com.
[55] Z. Yan, X. Cheng, T. Wang, X. Hong, G. Shao, C. Fu, Therapeutic potential for targeting Annexin A1 in fibrotic diseases, Genes Dis 9 (2022) 1493–1505. https://doi.org/10.1016/j.gendis.2022.05.038.
[56] L. Chen, S. Li, W. Li, LOX/LOXL in pulmonary fibrosis: potential therapeutic targets, J Drug Target 27 (2019) 790–796. https://doi.org/10.1080/1061186X.2018.1550649.
[57] J. Zhao, C. Jing, R. Fan, W. Zhang, Prognostic model of fibroblasts in idiopathic pulmonary fibrosis by combined bulk and single-cell RNA-sequencing, Heliyon 10 (2024). https://doi.org/10.1016/j.heliyon.2024.e34519.
[58] S. Réty, D. Osterloh, J.-P. Arié, S. Tabaries, J. Seeman, F. Russo-Marie, V. Gerke, A. Lewit-Bentley, Structural basis of the Ca 2+-dependent association between S100C (S100A11) and its target, the N-terminal part of annexin I, 2000.
[59] D. Schulz Torres, T.M. Freyman, I. V. Yannas, M. Spector, Tendon cell contraction of collagen-GAG matrices in vitro: Effect of cross-linking, Biomaterials 21 (2000) 1607–1619. https://doi.org/10.1016/S0142-9612(00)00051-X.
[60] M.B. Vaughan, G. Xu, T.L. Morris, P. Kshetri, J.X. Herwig, Predictable fibroblast tension generation by measuring compaction of anchored collagen matrices using microscopy and optical coherence tomography, Cell Adh Migr 13 (2019) 303–314. https://doi.org/10.1080/19336918.2019.1644855.
[61] J.E. Marturano, J.D. Arena, Z.A. Schiller, I. Georgakoudi, C.K. Kuo, Characterization of mechanical and biochemical properties of developing embryonic tendon, Proceedings of the National Academy of Sciences 110 (2013) 6370 LP – 6375. https://doi.org/10.1073/pnas.1300135110.
[62] A. Saraswathibhatla, D. Indana, O. Chaudhuri, Cell-extracellular matrix mechanotransduction in 3D HHS Public Access, Nat Rev Mol Cell Biol 24 (2023) 495–516. https://doi.org/10.1038/s415XX-XXX-XXXX-X.
[63] Y.A. Miroshnikova, S.A. Wickström, Mechanical Forces in Nuclear Organization, Cold Spring Harb Perspect Med 14 (2022). https://doi.org/10.1101/cshperspect.a039685.
[64] J. Garvin, J. Qi, M. Maloney, A.J. Banes, Novel System for Engineering Bioartificial Tendons and Application of Mechanical Load, Tissue Eng 9 (2003) 967–979. https://doi.org/10.1089/107632703322495619.
[65] M.Y. Pechanec, T.N. Boyd, K. Baar, M.J. Mienaltowski, Adding exogenous biglycan or decorin improves tendon formation for equine peritenon and tendon proper cells in vitro, BMC Musculoskelet Disord 21 (2020). https://doi.org/10.1186/s12891-020-03650-2.
[66] S. Eloy-Trinquet, H. Wang, F. Edom-Vovard, D. Duprez, Fgf signaling components are associated with muscles and tendons during limb development, Developmental Dynamics 238 (2009) 1195–1206. https://doi.org/https://doi.org/10.1002/dvdy.21946.

[67] T. Wang, P. Chen, M. Zheng, A. Wang, D. Lloyd, T. Leys, Q. Zheng, M.H. Zheng, In vitro loading models for tendon mechanobiology, Journal of Orthopaedic Research 36 (2018) 566–575. https://doi.org/10.1002/jor.23752.

[68] K.J. Livak, T.D. Schmittgen, Analysis of Relative Gene Expression Data Using Real-Time Quantitative PCR and the 2−ΔΔCT Method, Methods 25 (2001) 402–408. https://doi.org/10.1006/meth.2001.1262.

[69] M.A. Bonnin, C. Laclef, R. Blaise, S. Eloy-Trinquet, F. Relaix, P. Maire, D. Duprez, Six1 is not involved in limb tendon development, but is expressed in limb connective tissue under Shh regulation, Mech Dev 122 (2005) 573–585. https://doi.org/10.1016/j.mod.2004.11.005.

[70] M. Bléher, B. Meshko, I. Cacciapuoti, R. Gergondey, Y. Kovacs, D. Duprez, A. L'Honoré, E. Havis, Egr1 loss-of-function promotes beige adipocyte differentiation and activation specifically in inguinal subcutaneous white adipose tissue, Sci Rep 10 (2020) 1–15. https://doi.org/10.1038/s41598-020-72698-w.

Figure Legends

Figure 1: Generation of 3D-hASC constructs using a Flexcell bioreactor. A) Human adipose stromal cells are isolated from lipoaspirates and amplified before seeding. The cells are embedded in a 3.5% collagen hydrogel and deposited between the two anchor points. The polymerization is performed by maintaining the vacuum and at 37°C for 2 hours. The vacuum is then broken and the 3D-hASC constructs are kept in the incubator for 48 hours before starting the experiments. Scale bar 100µm. B) 3D-hASC constructs were cultured for 21 days and C) Diameters were measured from constructs at Day 0 (n=11), Day 7 (n=15), Day 14 (n=14) and Day 21 (n=19). Each color represents a set of experiments. 4 independent experiments were performed with 3<n<8 biological replicates for each experiment. The p-values were obtained using the Mann-Whitney test. Asterisks * indicate the p-values of 3D-hASCs construct diameter compared to each following stage, ****P<0.001. Scale bars 500µm. D) 3D-hASC construct total cell number was counted at Day 0 (n=9), Day 7 (n=9), Day 14 (n=9) and Day 21 (n=9). Each color represents a set of experiments. 3 independent experiments were performed with n=3 biological replicates for each experiment. The p-values were obtained using the Mann-Whitney test. Asterisks * indicate the p-values of 3D-hASCs construct cell number compared to each following stage, ** P<0.01, ****P<0.0001. E) Longitudinal sections of 3D-hASC constructs were performed at Day 4 and stained with DAPI/Phalloidin to visualize cellular and nuclear shape. Scale bars: 50 µm. F) Longitudinal sections of 3D-hASC constructs were performed on Day 0, Day 2, Day 4, Day 7, Day 14 and Day 21. The angles of 15 cells were measured on a minimum of 3 constructs per time point and compared to the axis of tension. Each dot represents the mean of 15 values per 3D-hASC construct. Asterisks * indicate the p-values of 3D-hASCs construct cell number compared to each following stage, * P<0.05, **P<0.01. G) After 0, 2, 4, 7, 14 and 21 Days of culture, 3D-hASC constructs were used for mRNA purification. mRNA expression levels of *COL1A1* were analysed by RT-qPCR. H) 3D-hASC constructs at Day 4 were transversally cryo-sectioned. 12 µm sections were hybridized with the DIG-labeled antisense probes for *COL1A1*. Scale bar: 250µm. I) 3D-hASC constructs at Day 4 Day 0, Day 7, Day 14 and Day 21 were transversally cryo-sectioned. 12 µm sections were hybridized with the DIG-labeled antisense probes for *COL1A1*. Scale bars: 50µm.

Figure 2: 3D-hASC constructs express tendon genes. A) After 0, 2, 4, 7, 14 and 21 Days of culture, 3D-hASC constructs were used for mRNA purification. mRNA expression levels of *SCX* were analysed by RT-qPCR. B) 3D-hASC constructs at Day 0, Day 7, Day 14 and Day 21

were transversally cryo-sectioned. 12 µm sections were hybridized with the DIG-labeled antisense probes for *SCX*. Scale bars: 50µm. After 0, 2, 4, 7, 14 and 21 Days of culture, 3D-hASC constructs were used for mRNA purification. mRNA samples were analysed by RT-qPCR for C) *MKX* D) *TNMD* and E) *THBS2*. F) 3D-hASC constructs at Day 0, Day 7, Day 14 and Day 21 were transversally cryo-sectioned. 12 µm sections were hybridized with the DIG-labeled antisense probes for *THBS2.* Scale bars 50µm. mRNA expression levels of G) *TM4FS1*, H) *ANXA1*, I) *S100A10*, J) *COL2A1* were analysed by RT-qPCR. Transcripts are shown relative to the level of *YWHAZ* transcripts. The relative mRNA levels were calculated using the $2^{\wedge-\Delta\Delta Ct}$ method, with control being normalized to 1. Each color represents a set of experiments. 8 independent experiments were performed with 14 < n < 29 3D-hASCs construct generated for each step (n=29 at Day 0, n=19 at Day 2, n=18 at Day 4, n=25 at Day 7, n=17 at Day 14 and n=16 at Day 21). The C_T values shown for tendon genes and *YWHAZ* represent the average of all C_T values obtained for each time point. Error bars represent the mean + standard deviations. The p-values were obtained using the Mann-Whitney test. Asterisks * indicate the p-values of gene expression levels in 3D-hASC constructs compared to the first Day of gene detection *P<0.05, **P<0.01, *** P<0.001, **** P<0.0001.

Figure 3: 3D-hASC construct Young's modulus increased along time. A) 3D-hASC constructs are fixed on a 3D-printed support maintained in agarose gel. B) 3D-hASC constructs are placed in an appropriate channel according to their diameter and fixed using dissection pins inserted into the anchor stems and agarose. C) The one-piece optical probe of the nanoindenter is composed of an optical fiber, a cantilever and a spherical tip. After an approach phase, the tip touches the sample and indent it. The cantilever bending is detected by the optical fiber. D) Force as a function of cantilever base displacement for a typical indentation. Inset: Cantilever base displacement is applied at constant rate of 10µm.s-1. E) Force as a function of indentation for a typical indentation curve. Hertz contact fit (red) is applied over a 1 µm indentation. F) Evolution of effective Young's modulus along culture time in 3D-constructs without cells and seeded with hASCs. For 3D-no cell constructs without cells, each dot represents the mean of five measurements performed on one construct. Indentation experiments were performed at Day 0 (n=8), Day 7 (n=6), Day 14 (n=6) and Day 21 (n=12). Each color represents a set of experiments. 2 independent experiments were performed with 3<n<6 biological replicates for each experiment. For 3D-hASC constructs, each dot represents the mean of five measurements performed on one 3D-hASCs construct. Indentation experiments were performed at Day 0 (n=17), Day 7 (n=17), Day 14 (n=13) and Day 21 (n=14). Each color represents a set of experiments. 5 independent experiments were performed with 3<n<8 biological replicates for each experiment. The p-values were obtained using the Mann-Whitney test. Asterisks * indicate the p-values of Young's modulus levels (kPa) in 3D-hASC constructs compared to each following stage, ***P<0.001, ****P<0.0001. # indicates the p-values of Young's modulus levels (kPa) in 3D-no cell constructs compared to 3D-hASC constructs, ###P<0.001, ####P<0.0001.

Figure 4: Extra-cellular matrix gene expression was highly increased during 3D-hASC construct development. After 0, 2, 4, 7, 14 and 21 Days of culture, 3D-hASC constructs were used for mRNA purification. mRNA expression levels of tendon-associated collagens A) *COL6A3*, B) *COL14A1* and extracellular matrix protein coding genes C) *DCN*, D) *POSTN,* E) *DPT* and F) *LOX* were analysed by RT-qPCR. Transcripts are shown relative to the level of *YWHAZ* transcripts. The relative mRNA levels were calculated using the $2^{\wedge-\Delta\Delta Ct}$ method, with control being normalized to 1. Each color represents a set of experiments. 8 independent experiments were performed with 14 < n < 29 3D-hASCs construct generated for each step (n=29 at Day 0, n=19 at Day 2, n=18 at Day 4, n=25 at Day 7, n=17 at Day 14 and n=16 at Day

21). The C_T values shown for tendon genes and *YWHAZ* represent the average of all C_T values obtained for each time point. Error bars represent the mean + standard deviations. The p-values were obtained using the Mann-Whitney test. Asterisks * indicate the p-values of gene expression levels in 3D-hASC constructs compared to the first Day of gene detection *P<0.05, **P<0.01, *** P<0.001, **** P<0.0001.

Figure 5: Viscoelastic properties of human 3D-hASC constructs change over the course of the culture. A) Schematic of a force relaxation experiment. In open loop, the base of the cantilever is fixed while relaxation takes place. B) Typical curve showing force as a function of indentation during loading, relaxation and unloading phase. Inset: Indentation as a function of time. C) Force as a function of cantilever base displacement for a typical indentation. Inset: Cantilever base displacement is applied at constant rate of 10µm.s-1. D) Force as a function time. Force peaks at a value Fmax and reaches is close to a plateau after 10s of relaxation. Frelax is defined as the force at this instant. E) Percentage of stress relaxation ((Fmax – Ft=10 sec) / Fmax)) x100 during the first 10 seconds of relaxation, after different periods of cell culture. For 3D-no cell constructs without cells, each dot represents the mean of five measurements performed on one construct. Indentation experiments were performed at Day 0 (n=8), Day 7 (n=6), Day 14 (n=6) and Day 21 (n=12). Each color represents a set of experiments. 2 independent experiments were performed with 3<n<6 biological replicates for each experiment. For 3D-hASC constructs, indentation experiments were performed at Day 0 (n=17), Day 7 (n=17), Day 14 (n=13) and Day 21 (n=14). Each color represents a set of experiments. 5 independent experiments were performed with 3<n<8 biological replicates for each experiment. The p-values were obtained using the Mann-Whitney test. Asterisks * indicates the p-value of 3D-hASCs construct relaxation compared to each following stage; *P<0.05; @ indicates the p-value of 3D-no cell construct relaxation compared to each following stage, @P<0.05; # indicates the p-value of in 3D-no cell constructs compared to 3D-hASC constructs, ###P<0.001, ####P<0.0001.

Figure 6: Cellular organization in 3D engineered 3D-hASCs. A) 3D-hASCs transverse section representation. B) Transverse sections of 3D-hASC constructs were performed on Day 0, Day 2, Day 4, Day 7, Day 14 and Day 21 of culture and stained with DAPI/Phalloidin to visualize cell organization within the 3D-hASC constructs. From Day 2, 3D-hASC constructs are composed of two cell populations, one at the centre and the other at the periphery, forming a ring. D) Cell density was counted at the centre and the ring of 3D-hASC constructs at Day 0 (n=18), Day 2 (n=12), Day 4 (n=10), Day 7 (n=15), Day 14 (n=12) and Day 21 (n=9). The p-values were obtained using the Mann-Whitney test compared to each following stage. Asterisks * indicate the p-values of cell number at the centre, *** P <0.001, **** P<0.0001; # indicate the p-values of cell number at the ring, #### P <0.0001; Scale bars 100µm.

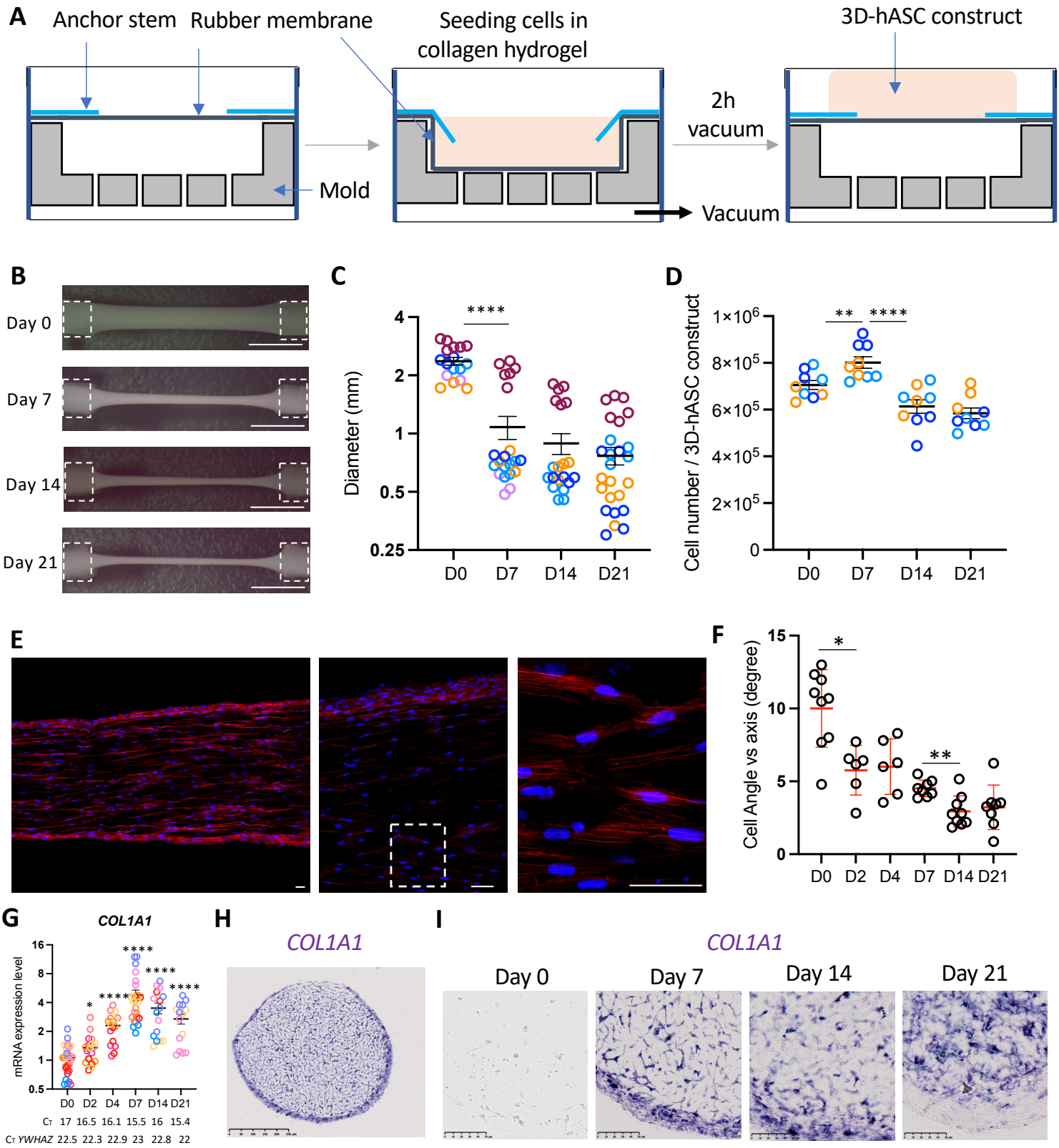
A
Anchor stem
Rubber membrane
Seeding cells in collagen hydrogel
3D-hASC construct
2h vacuum
Mold
Vacuum
B
Day 0
Day 7
Day 14
Day 21
C
Diameter (mm)
D0 D7 D14 D21
D
Cell number / 3D-hASC construct
D0 D7 D14 D21
E
F
Cell Angle vs axis (degree)
D0 D2 D4 D7 D14 D21
G
COL1A1
mRNA expression level
D0 D2 D4 D7 D14 D21
CT 17 16.5 16.1 15.5 16 15.4
CT YWHAZ 22.5 22.3 22.9 23 22.8 22
H
COL1A1
I
COL1A1
Day 0
Day 7
Day 14
Day 21

Figure 1

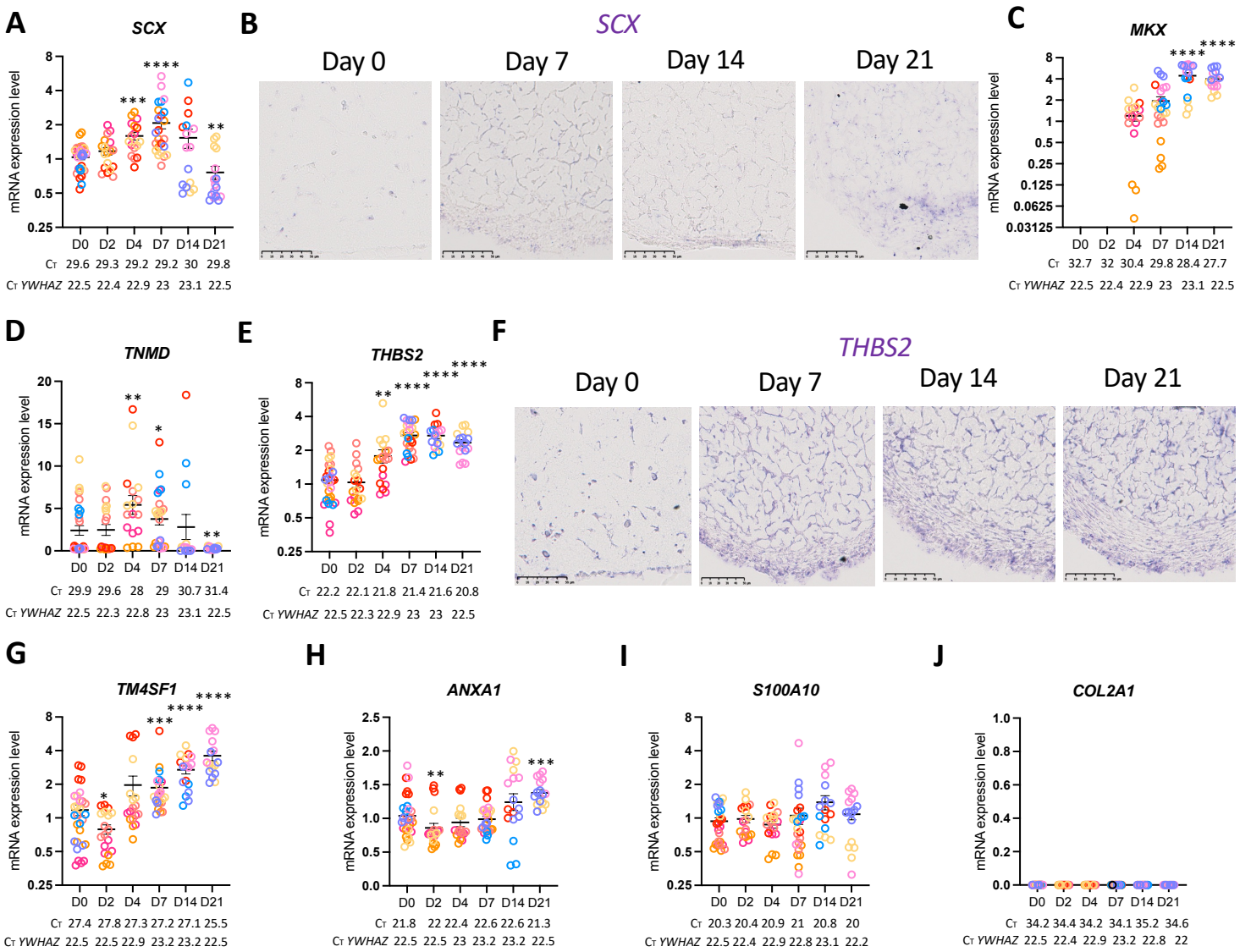
A
SCX
mRNA expression level
D0 D2 D4 D7 D14 D21
CT 29.6 29.3 29.2 29.2 30 29.8
CT YWHAZ 22.5 22.4 22.9 23 23.1 22.5
B
SCX
Day 0
Day 7
Day 14
Day 21
C
MKX
mRNA expression level
D0 D2 D4 D7 D14 D21
CT 32.7 32 30.4 29.8 28.4 27.7
CT YWHAZ 22.5 22.4 22.9 23 23.1 22.5
D
TNMD
mRNA expression level
D0 D2 D4 D7 D14 D21
CT 29.9 29.6 28 29 30.7 31.4
CT YWHAZ 22.5 22.3 22.8 23 23.1 22.5
E
THBS2
mRNA expression level
D0 D2 D4 D7 D14 D21
CT 22.2 22.1 21.8 21.4 21.6 20.8
CT YWHAZ 22.5 22.3 22.9 23 23 22.5
F
THBS2
Day 0
Day 7
Day 14
Day 21
G
TM4SF1
mRNA expression level
D0 D2 D4 D7 D14 D21
CT 27.4 27.8 27.3 27.2 27.1 25.5
CT YWHAZ 22.5 22.5 22.9 23.2 23.2 22.5
H
ANXA1
mRNA expression level
D0 D2 D4 D7 D14 D21
CT 21.8 22 22.4 22.6 22.6 21.3
CT YWHAZ 22.5 22.5 23 23.2 23.2 22.5
I
S100A10
mRNA expression level
D0 D2 D4 D7 D14 D21
CT 20.3 20.4 20.9 21 20.8 20
CT YWHAZ 22.5 22.4 22.9 22.8 23.1 22.2
J
COL2A1
mRNA expression level
D0 D2 D4 D7 D14 D21
CT 34.2 34.4 34.2 34.1 35.2 34.6
CT YWHAZ 22.5 22.4 22.9 23.2 22.8 22

Figure 2

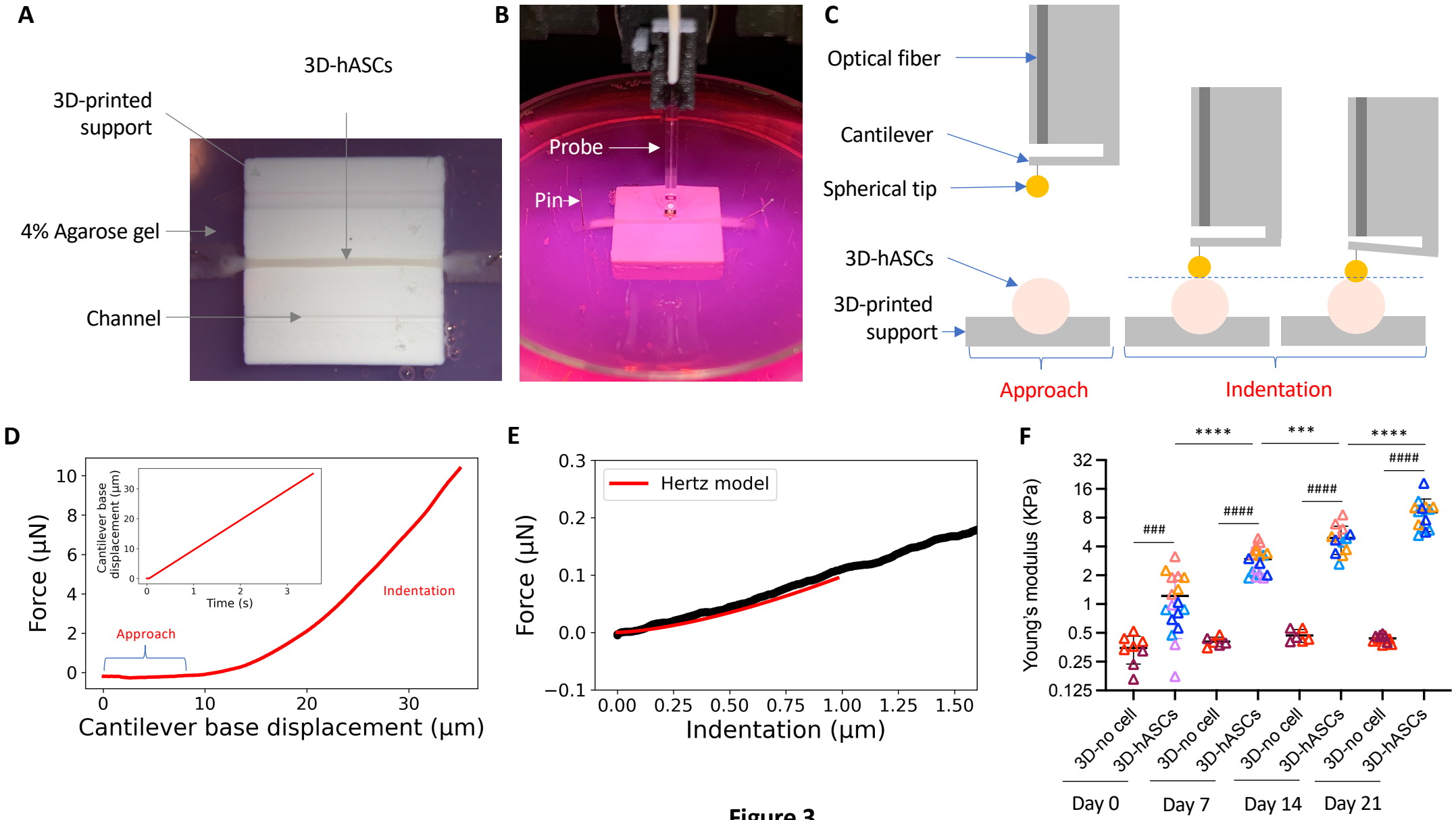
A
3D-hASCs
3D-printed support
4% Agarose gel
Channel
B
Probe
Pin
C
Optical fiber
Cantilever
Spherical tip
3D-hASCs
3D-printed support
Approach
Indentation
D
Force (µN)
Cantilever base displacement (µm)
Cantilever base displacement (µm)
Time (s)
Approach
Indentation
E
Hertz model
Force (µN)
Indentation (µm)
F
Young's modulus (KPa)
3D-no cell
3D-hASCs
Day 0
Day 7
Day 14
Day 21
****
***
****
###
####
####
####

Figure 3

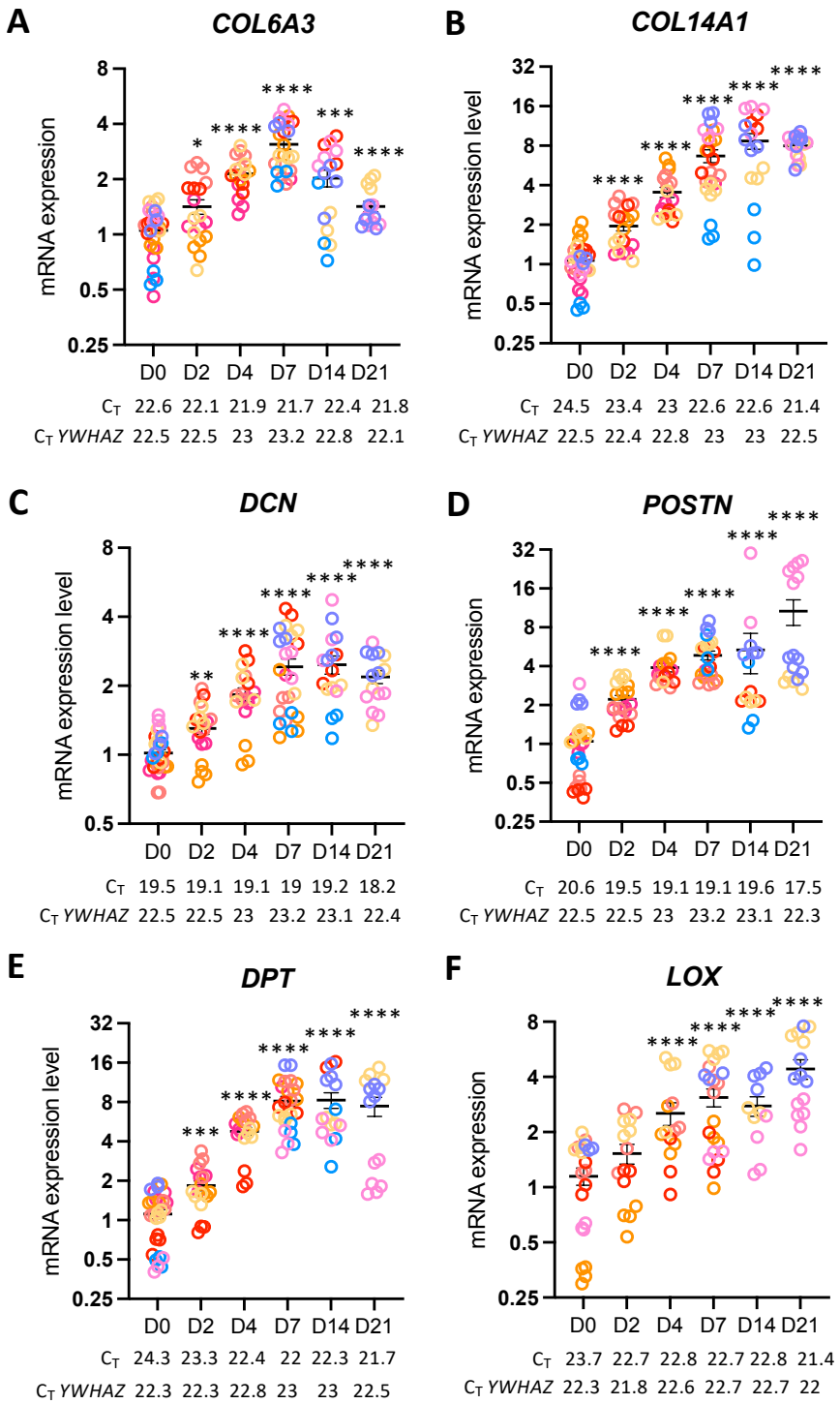
A
COL6A3
mRNA expression
8
4
2
1
0.5
0.25
D0 D2 D4 D7 D14 D21
CT 22.6 22.1 21.9 21.7 22.4 21.8
CT YWHAZ 22.5 22.5 23 23.2 22.8 22.1
B
COL14A1
mRNA expression level
32
16
8
4
2
1
0.5
0.25
D0 D2 D4 D7 D14 D21
CT 24.5 23.4 23 22.6 22.6 21.4
CT YWHAZ 22.5 22.4 22.8 23 23 22.5
C
DCN
mRNA expression level
8
4
2
1
0.5
D0 D2 D4 D7 D14 D21
CT 19.5 19.1 19.1 19 19.2 18.2
CT YWHAZ 22.5 22.5 23 23.2 23.1 22.4
D
POSTN
mRNA expression
32
16
8
4
2
1
0.5
0.25
D0 D2 D4 D7 D14 D21
CT 20.6 19.5 19.1 19.1 19.6 17.5
CT YWHAZ 22.5 22.5 23 23.2 23.1 22.3
E
DPT
mRNA expression level
32
16
8
4
2
1
0.5
0.25
D0 D2 D4 D7 D14 D21
CT 24.3 23.3 22.4 22 22.3 21.7
CT YWHAZ 22.3 22.3 22.8 23 23 22.5
F
LOX
mRNA expression
8
4
2
1
0.5
0.25
D0 D2 D4 D7 D14 D21
CT 23.7 22.7 22.8 22.7 22.8 21.4
CT YWHAZ 22.3 21.8 22.6 22.7 22.7 22

Figure 4

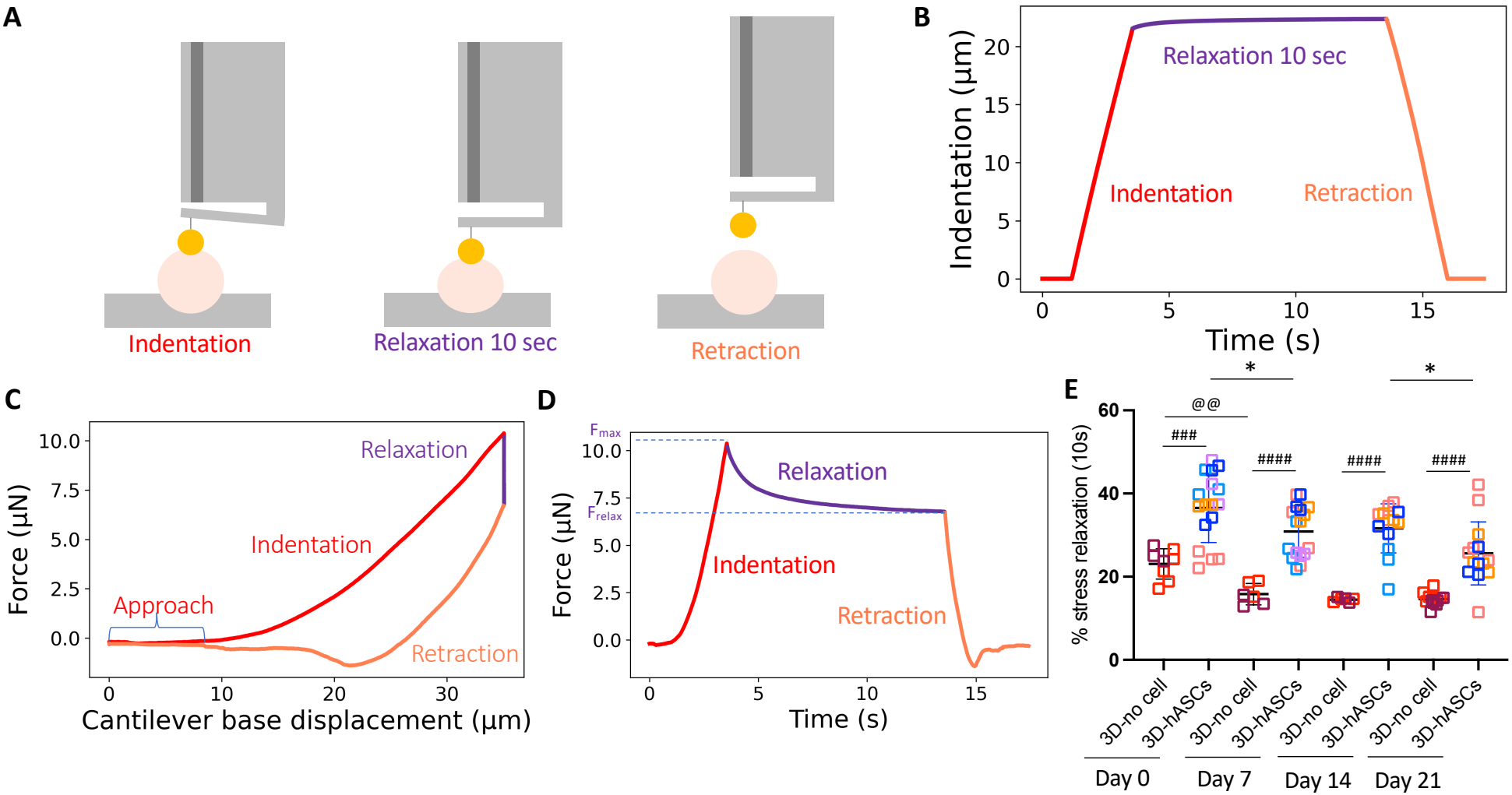
A
Indentation
Relaxation 10 sec
Retraction
B
Indentation (µm)
Time (s)
Relaxation 10 sec
Indentation
Retraction
C
Force (µN)
Cantilever base displacement (µm)
Approach
Indentation
Relaxation
Retraction
D
Force (µN)
Time (s)
Fmax
Frelax
Relaxation
Indentation
Retraction
E
% stress relaxation (10s)
@@
###
####
3D-no cell
3D-hASCs
Day 0
Day 7
Day 14
Day 21

Figure 5

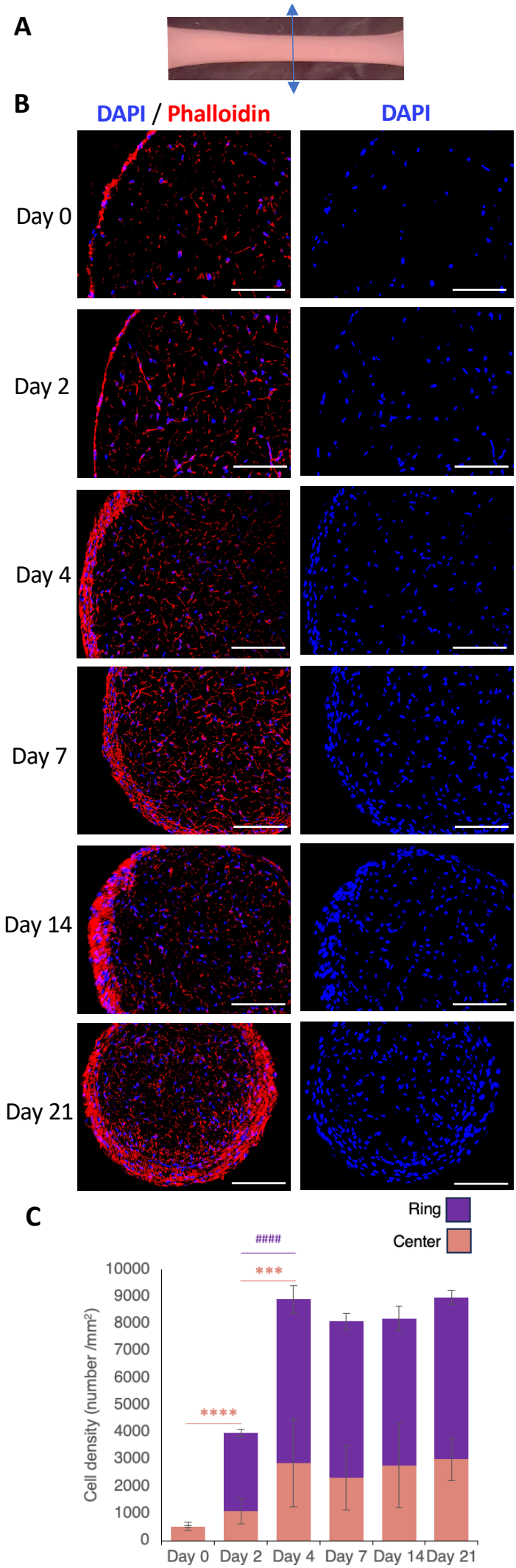
A
B
DAPI / Phalloidin
DAPI
Day 0
Day 2
Day 4
Day 7
Day 14
Day 21
C
Ring
Center
####
***
****
Cell density (number /mm²)
10000
9000
8000
7000
6000
5000
4000
3000
2000
1000
0
Day 0
Day 2
Day 4
Day 7
Day 14
Day 21

Figure 6